

Model for Nitric oxide and its dayglow emission in the Martian upper atmosphere using NGIMS/MAVEN measured neutral and ion densities

Susarla Raghuram^{a,b,c,*}, Anil Bhardwaj^a and Maneesha Dharwan^{a,d}

^aPhysical Research Laboratory, Ahmedabad, 380009, India.

^bLaboratory for Atmospheric and Space Physics, University of Colorado Boulder, Boulder, CO, USA.

^cSpace and Planetary Science Center, Khalifa University of Science and Technology, Abu Dhabi, UAE.

^dMaulana Azad National Institute of Technology Bhopal, M. P., India.

ARTICLE INFO

Keywords:

Mars, Atmosphere
Abundances, atmospheres
Atmospheres, chemistry
Atmospheres, composition
Aeronomy

ABSTRACT

A comprehensive study of Nitric oxide (NO) chemistry in the Martian upper atmosphere is restricted due to the lack of requisite measurements. NO is an abundant form of odd nitrogen species in the Martian lower atmosphere and its density depends on several photochemical processes. We have developed a photochemical model to study the NO density in the dayside of Martian upper atmosphere by accounting for various production and loss mechanisms. By utilizing the Neutral Gas and Ion Mass Spectrometer (NGIMS) on-board Mars Atmosphere and Volatile Evolution (MAVEN) mission measured neutral and ion densities during deep dip 8 and 9 campaigns, we modelled NO number density in the Martian sunlit upper atmosphere for the altitudes between 120 and 200 km. The modelled NO densities are employed to calculate NO (1,0) γ band emission intensity profiles in the dayside upper atmosphere of Mars. The calculated NO density and its γ band intensity profiles are found to be consistent with Imaging Ultraviolet Spectrograph (IUVS) onboard MAVEN observations and also with other modelling studies. We found that the local CO₂ and N₂ density variations can lead to a change in NO density and consequently its dayglow intensity by a factor of 2 to 5. Since NO is a trace constituent and also its dayglow emissions are strongly obscured by CO Cameron band emissions, we suggest that the derivation of NO number density based on our approach can constrain its abundance in the dayside upper atmosphere of Mars. More observations of (1-0) γ band emission along with modelling will help to study the global distribution of NO in the Martian atmosphere.

1. Introduction

Many in-situ and remote observations along with theoretical studies were carried out to understand the composition and energetics of the Martian upper atmosphere (Nier and McElroy, 1977; Krasnopolsky, 1993; Bertaux et al., 2005b; Withers, 2006; González-Galindo et al., 2009; Bougher et al., 2015a; Mahaffy et al., 2015; Bhardwaj et al., 2016, 2017). However, the study of minor neutrals in Martian upper atmosphere is still sparse due to lack of several key chemical reaction parameters and insufficient measurements from remote and in-situ observations. Nitric oxide (hereafter NO) is a minor species and its density in the dayside of Martian upper atmosphere is not well constrained. Several studies have shown that though the abundance of this species is in parts per million by volume in the thermosphere of Earth, but can play a significant role in driving the chemistry and thermal balance of the upper atmosphere (Barth, 1964; Norton and Barth, 1970; Eparvier and Barth, 1992; Barth et al., 2003; Bharti et al., 2019). Due to its lowest ionization potential (9.26 eV) compared to any other atmospheric species, NO quickly does exchange the charge with O₂⁺ and causes NO⁺ as the dominant ion at the lower altitudes around 80 km in the Martian ionosphere (Fox, 2004). Hence, this species plays a significant role in the thermospheric energy budget and also in determining

the ionospheric composition in the Martian atmosphere. But the study of NO global distribution and its role in the energy budget of Martian thermosphere is limited due to the lack of adequate in-situ and remote observations.

The global distribution of NO in the Martian upper atmosphere can be studied from the remote observations of its γ band emissions in the ultraviolet region. But the observation of these band emissions and the derivation of NO density in sunlit Martian upper atmosphere is challenging due to the presence of intense CO Cameron bands in the same emitting wavelength region. Spectroscopy for the Investigation of the Characteristics of the Atmosphere of Mars (SPICAM) experiment on-board Mars Express (MEX) spacecraft (SPICAM/MEX) and Imaging Ultraviolet Spectrograph (IUVS) on-board Mars Atmosphere and Volatile Evolution (MAVEN) satellite (IUVS/MAVEN) have played a key role in studying the NO distribution in the night side of Martian upper atmosphere via γ (225–270 nm) and δ (190–240 nm) band emission observations (Bertaux et al., 2005a,b; Cox et al., 2008; Gagné et al., 2013; Stevens et al., 2019). Recently, Stevens et al. (2019) reported first-ever NO dayglow (1,0) γ band emission (A² Σ^+ -X² Π) in the IUVS/MAVEN spectra, which were observed during 6–8 April 2016 at solar zenith angle (SZA) 75°. The measured NO (1-0) γ band limb radiance profiles have been used to retrieve NO density in the altitude range 80 to 120 km. Above 120 km, the retrieval process becomes tedious due to higher intensity of CO Cameron band emission which is about 50 times brighter than NO γ band emission.

*Corresponding author

✉ raghuramsusarla@gmail.com (S. Raghuram)

ORCID(S): 0000-0002-1309-2499 (S. Raghuram); 0000-0003-1693-453X (A. Bhardwaj); 0000-0001-6917-4963 (M. Dharwan)

Regarding in-situ measurements, Upper Atmosphere Mass Spectrometer (UAMS) instruments on-board Viking 1 and 2 landers made first-ever in-situ NO number density measurements in the dayside Martian upper atmosphere on 20 July 1976 (solar longitude, $L_s = 97^\circ$) and 3 September 1976 ($L_s = 118^\circ$), respectively, at three to four different altitudes between 110 and 150 km. (McElroy et al., 1976; Nier and McElroy, 1977). By accounting for the important photochemical reaction network, Fox (1993) modelled NO number density and found that their calculated density is smaller by a factor of 2–3 compared to the Viking measurement at an altitude around 115 km. The reason for the discrepancy between the Fox (1993) modelled and Viking observed NO densities has not been understood and remained as a long-standing issue due to the lack of adequate measurements. After nearly four decades, since the Viking landers experiments, the Neutral Gas and Ion Mass Spectrometer (NGIMS) on-board MAVEN mission (NGIMS/MAVEN) measured NO number densities in the Martian upper atmosphere (Mahaffy et al., 2015; Vogt et al., 2017). However, the NGIMS/MAVEN measured NO densities are an order of magnitude higher than those predicted by earlier theoretical models. As pointed by Stevens et al. (2019), the contamination in the measurement, which arises due to the recombination of atomic nitrogen and atomic oxygen within the instrument, could be a reason for the higher reported NO densities.

As discussed before, there are several constrains to study NO number density in the dayside Martian upper atmosphere for the both in-situ (Viking 1, 2, and NGIMS/MAVEN) and remote (SPICAM/MEx and IUVS/MAVEN) observations. In this paper, we present an approach of calculating the NO number density in the dayside Martian upper atmosphere by incorporating NGIMS/MAVEN measured neutral (CO_2 , N_2 , and O) and ion (NO^+ , O_2^+ and CO_2^+) number densities in the photochemical network. We show that our approach can be used to constrain the NO density in the altitude range between 120 and 200 km based on the MAVEN measurements during deep dip 8 and 9 campaigns. We have also calculated dayside NO (1-0) γ limb intensity profiles from our modelled NO densities and compared them with the IUVS/MAVEN observations. The methodology adopted in this work is explained in Section 2. The results obtained analysis are presented in Section 3. We have discussed various factors which can influence our modelled NO density profiles in Section 4. This work has been summarized and conclusions are drawn in Section 5.

2. Methodology

The neutral and ion number densities are taken from the dayside NGIMS/MAVEN inbound measurements for SZA smaller than 60° during deep dip 8 and 9 campaigns. To extract the neutral and ion density profiles, we utilized level 2 data (L2), version 7 (8), revision 3 (1) data for deep dip 8 (9) campaign. Additional details of the L2 data product are available in Benna and Elrod (2018) and the data can be accessed from a web link (<https://pds-atmospheres.nmsu.edu>).

We chose only those orbits of MAVEN deep dip 8 and 9 campaigns where both neutral and ion densities are measured. The obtained densities are interpolated over a uniform grid of 1 km from MAVEN's periapsis altitude to 200 km. Table 1 summarizes the MAVEN observational conditions, such as observation period, orbit numbers, L_s , and the variation in SZA and latitude during orbits, during deep dip 8 and 9 campaigns.

The chemical network considered in this work is based on the compilation of Fox and Sung (2001) with updated rate coefficients from McElroy et al. (2013). These chemical reactions are tabulated in Table 2. The electron temperature, which determines the dissociative recombination rate of ions, is taken from Ergun et al. (2015). Using the Analytical yield spectrum (AYS) approach, we calculated the suprathermal electron flux and electron impact dissociation rate of N_2 in the Martian upper atmosphere. More details of degradation of solar flux and the calculation of suprathermal electron flux using AYS method can be found in our earlier work (Bhardwaj et al., 1990; Bhardwaj et al., 1996; Bhardwaj, 1999; Jain and Bhardwaj, 2011; Jain and Bhardwaj, 2012; Bhardwaj and Jain, 2013; Raghuram and Bhardwaj, 2020). By assuming photochemical equilibrium condition and accounting for various production and loss mechanisms, we determined the NO, $\text{N}(^4\text{S})$ and $\text{N}(^2\text{D})$ number densities for the altitudes between 120 and 200 km. The effect of transport in calculating the number densities of these species is discussed in Section 4.

We have taken the fluorescence efficiency (g-factor) for NO (1,0) γ band emission as 2.68×10^{-6} photons s^{-1} molecule $^{-1}$ and all the photorates are scaled to heliocentric distance of 1.57 AU (Stevens et al., 2019). The Volume Emission Rate (VER), which is the number of photons scattered per unit volume per unit time, is calculated by multiplying the modelled NO number density with the g-factor. The limb emission intensity of this band is obtained by integrating the volume emission rate along the line of sight and converted into brightness in Rayleigh ($1 \text{ Rayleigh} = 10^6/4\pi \text{ photons cm}^{-2} \text{ sec}^{-1} \text{ sr}^{-1}$) using the following equation.

$$I = 2 \times 10^{-6} \int_0^\infty \text{VER}(r) dr \quad (1)$$

here r is the abscissa along the horizontal line of sight and $\text{VER}(r)$ is the volume emission rate (photons $\text{cm}^{-3} \text{ sec}^{-1}$) at a particular emission point r . The factor 2 multiplication in the above equation is due to the symmetry along the line of sight concerning the tangent point. While calculating the limb intensity, we assumed that the emission rate is constant along the local longitude/latitude. Other Martian species cannot absorb NO emissions along the line of sight due to low absorption cross section, hence the atmospheric absorption for this band emission can be neglected.

Table 1

The observational conditions of MAVEN deep dip 8 and 9 campaigns.

#DD ¹	Observation period	Orbits	SZA ²	Lat. ³	Ls ⁴
8	16–22 October 2017	5909–5947	22–40°	10°N–21°N	76°
9	24–30 April 2018	6936–6973	28–59°	19°S–52°S	165°

¹Deep dip; ²Solar zenith angle; ³Latitude; ⁴Solar longitude.

3. Results

The NGIMS/MAVEN measured neutral and ion densities profiles for orbit #5947 of deep dip 8 campaign are presented in Figure 1. In this Figure, we compared the NGIMS/MAVEN measured CO₂, N₂ and O density profiles with Fox (2004) modelled density profiles, which are constructed based on the Viking observations for solar minimum condition. It can be noticed in this figure that Fox (2004) modelled neutral density profiles are higher by a factor of 2 to 4 compared to NGIMS/MAVEN measured values.

Using the NGIMS/MAVEN measurements for orbit #5947, the modelled production and loss profiles of N(⁴S), N(²D), and NO are presented in the top and bottom panels of Figure 2, respectively. The calculated production rate profiles in the top panels of this Figure show that photodissociation of N₂ is the major source of N(⁴S) and N(²D) production, whereas the collisional reaction between N(²D) and CO₂ leads to the formation of NO. For the altitudes above 180 km, radiative decay of N(²D) also contributes significantly to the total formation of N(⁴S), whereas the collisional reaction between CO₂⁺ and N(⁴S) is also an important source mechanism in the total NO formation. It can be noticed in this Figure that the role of other chemical processes is small in the formation of N(⁴S), N(²D) and NO when compared to previously discussed major production mechanisms.

The modelled loss frequency profiles in the bottom panels of Figure 2 show that for the altitudes below 160 km, the total loss of N(⁴S) is mainly due to the collisions with NO, and above this distance it is removed by the collisions of O₂⁺ in the Martian upper atmosphere. The loss frequency of N(⁴S) by CO₂ collision is smaller by an order of magnitude or more compared to that of the previously discussed loss mechanisms which is due to small collisional rate coefficient (more than five order of magnitude smaller, see reactions R7, R8, and R10 in Table 2). For the altitudes below 180 km, the total loss of N(²D) is mainly due to the collisions with CO₂, which leads to the formation of NO, and above this altitude the radiative decay is the dominant loss mechanism that causes N(⁴S) formation. The loss of NO is mainly due to the collisions with N(⁴S) which leads to the formation of N₂. Several other reactions are also involved in the loss of these species but their contribution to the total loss frequency is small.

The modelled number density profiles of N(⁴S), N(²D) and NO for orbit #5947 of MAVEN deep dip 8 campaign are presented in Figure 3. Our modelled NO and N(⁴S) density

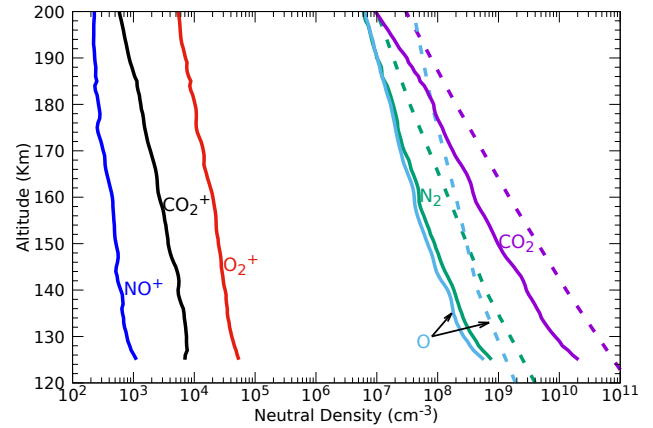


Figure 1: The NGIMS/MAVEN measured neutral and ion number density profiles for orbit #5947 of deep dip 8 campaign. The dashed curves with corresponding colours represent the neutral density profiles for solar minimum condition from Fox (2004).

profiles are lower and higher by a factor of 2 to 3, respectively, compared those of Fox (2004). Our modelled N(²D) density profile is closer to Fox (2004) calculated value for the altitude above 130 km. The reason for differences between these density profiles is discussed in Section 4.

We have employed the same approach in calculating the NO number density profiles for all the orbits of MAVEN deep dip 8 and 9 campaigns. Using the NGIMS/MAVEN measured neutral and ion number density for the orbits of deep dip 8 campaign (#5909 to #5947) and accounting for the previously discussed photochemical network of reactions, the modelled NO number density profiles are presented in Figure 4. We find that our modelled NO number density is varying over different orbits and this is mainly associated with the variability in the NGIMS/MAVEN measured neutral and ions density measurements. The variation in the calculated NO number density for different orbits is found to be small (by a factor of 2) at lower altitudes (around 120 km) and it is increasing with altitude (more than a factor of 2, see the gray shaded area in Figure 4). The calculated NO number density profiles for all the 32 orbits, i.e., from #6936 to #6973, of MAVEN deep dip 9 campaign are presented in Figure 5. In this case, the calculated NO density around 120 km altitude is about 10⁶ cm⁻³ and comparable to the derived value for the deep dip 8 campaign.

In Figure 6, we compared the calculated NO number density profiles during MAVEN deep dip 8 and 9 campaigns with IUVS/MAVEN retrieved value. The modelled average NO number density profile for deep dip 8 campaign is consistent with the IUVS/MAVEN retrieved value at around 125 km altitude. Stevens et al. (2019) modelled NO density profiles in the altitude range 80 and 160 km at SZA 44° and 75° for IUVS and Viking observational conditions, respectively (see dashed red and blue curves in Figure 6). Our modelled NO number density profiles are also consistent with the

Table 2

Production and loss reactions of NO, N(⁴S) and N(²D) for the altitudes above 120 km in the Martian upper atmosphere.

No.	Reaction	Rate coefficient (cm ³ sec ⁻¹ or sec ⁻¹)	Reference
R1	N(² D) + CO ₂ → NO + CO	3.6×10 ⁻¹³	Herron (1999)
R2	N(² D) + O → N(⁴ S) + O	6.90×10 ⁻¹³	Fell et al. (1990)
R3	N(² D) + N ₂ → N(⁴ S) + N ₂	1.70×10 ⁻¹⁴	Herron (1999)
R4	N(² D) + NO → N(⁴ S) + NO	6.70×10 ⁻¹¹	Fell et al. (1990)
R5	N(² D) + O ₂ ⁺ → NO ⁺ + O	1.80×10 ⁻¹⁰	Goldan et al. (1966)
R6	N(² D) + e _{th} → N(⁴ S) + O	3.86×10 ⁻¹⁰ (T _e /300) ^{0.81}	Berrington and Burke (1981)
R7	N(⁴ S) + CO ₂ → NO + CO	1.7×10 ⁻¹⁶	Fox and Sung (2001)
R8	N(⁴ S) + NO → N ₂ + O	3.38×10 ⁻¹¹ (300/T _n) ^{0.17} exp(-2.8/T _n)	McElroy et al. (2013)
R9	N(⁴ S) + CO ₂ ⁺ → NO + CO ⁺	3.40×10 ⁻¹⁰	Scott et al. (1998)
R10	N(⁴ S) + O ₂ ⁺ → NO ⁺ + O	1.80×10 ⁻¹⁰	McElroy et al. (2013)
R11	NO ⁺ + e _{th} → N(⁴ S) + O	0.60×10 ⁻⁷ (300/Te) ^{0.5}	Vejby-Christensen et al. (1998)
R12	NO ⁺ + e _{th} → N(² D) + O	3.40×10 ⁻⁷ (300/Te) ^{0.5}	Vejby-Christensen et al. (1998)
R13	NO + CO ₂ ⁺ → NO ⁺ + CO ₂	1.2 ×10 ⁻¹⁰	McElroy et al. (2013)
R14	NO + O ₂ ⁺ → NO ⁺ + O ₂	4.6 ×10 ⁻¹⁰	McElroy et al. (2013)
R15	N ₂ + hν → N(⁴ S) + N(⁴ S)	Calculated	This work
R16	N ₂ + hν → N(² D) + N(⁴ S)	Calculated	This work
R17	N ₂ + e _{ph} → N(⁴ S) + N(⁴ S)	Calculated	This work
R18	N ₂ + e _{ph} → N(² D) + N(⁴ S)	Calculated	This work
R19	N ₂ + O ₂ ⁺ → NO ⁺ + NO	2.0 ×10 ⁻¹⁸	Matsuoka et al. (1981)
R20	N(² D) → N(⁴ S) + hν	2.78 ×10 ⁻⁵	Tachiev and Froese Fischer (2002)

hν is photon, e_{ph} is photoelectron and e_{th} is thermal electron; T_n and T_e are neutral and electron temperatures, respectively.

Stevens et al. (2019) modelled profiles in the altitude range 120 to 160 km.

Our calculations in Figure 2 show that N₂ and CO₂ play a crucial role in determining the NO density in the Martian upper atmosphere. Hence, we studied the variation in our modelled NO density with respect to the changes in MAVEN measured CO₂ and N₂ densities. It can be noticed in Figure 7 that both the CO₂ and N₂ densities locally vary about a factor of 2 to 5 during deep dip 8 and 9 campaigns in the altitude range 120 to 200 km (see the shaded areas in figure 7). Due to significant variability in the measured densities, it is difficult to describe the impact of CO₂ and N₂ on NO for each orbit of both deep dip 8 and 9 campaigns. Hence, we chose two orbits for each campaign to demonstrate the impact of MAVEN measurements on the modelled NO density. As shown in the top panel of Figure 7, the MAVEN measured CO₂ and N₂ densities for orbit #5943 are higher compared to those for #5947 at the altitudes below 165 km and above this radial distance it is opposite. This cross over in the measured CO₂ and N₂ density profiles is also reflected in our modelled NO profiles for the corresponding orbits at 165 km altitude (see solid and dashed purple lines in the top panel of Figure 7). Similarly, as shown in the bottom panel of this figure, the MAVEN measured CO₂ and N₂ densities for orbits #6937 are higher compared to those for #6949 for deep dip 9 campaign in the altitude range 120 to 200 km. The higher densities of CO₂ and N₂ lead to larger production of NO which is reflected in the modelled NO density for orbit #6937. These calculations suggest that the change in CO₂ and N₂ densities directly can influence the NO density in the Martian upper atmosphere.

By utilizing the corresponding modelled NO number densities, the calculated limb intensity profiles for NO (1,0) γ band for the MAVEN deep dip 8 and 9 campaigns are presented in Figures 8 and 9, respectively. The calculated NO (1,0) γ band limb intensity is found to vary between 90 and 200 R (between 100 and 300 R) at the MAVEN periapsis altitude around 120 km during MAVEN deep dip 8 (9) campaign. We compared our calculated NO (1, 0) γ limb intensity profiles with and IUVS/MAVEN observation in Figure 10. Our calculated mean limb intensities for deep dip 8 and 9 campaigns around 120 km altitude are found to be consistent with the IUVS/MAVEN observation.

4. Discussion

During the deep dip campaigns, NGIMS/MAVEN measured both neutral and ion densities at the altitudes as low as 125 km, whereas the regular measurements cover the altitudes above 150 km. This possibility enabled us to calculate NO number density at the lower altitudes which is not possible for other measurements. Out of the total nine MAVEN deep dip campaigns so far, deep dip 2, 8, and 9 campaigns are occurred on the dayside. Recently, Cui et al. (2020) also used the NGIMS neutral and ion density measurements to constrain the NO density in the dayside Martian upper atmosphere, specifically for the deep dip 2 campaign during 17-22 April 2015 with a periapsis altitude of 130 km and appropriate for the subsolar condition. By neglecting transport, these authors carried out time-dependent calculations at a fixed altitude of 160km to investigate the diurnal variation under the influences of both dayside solar radiation and

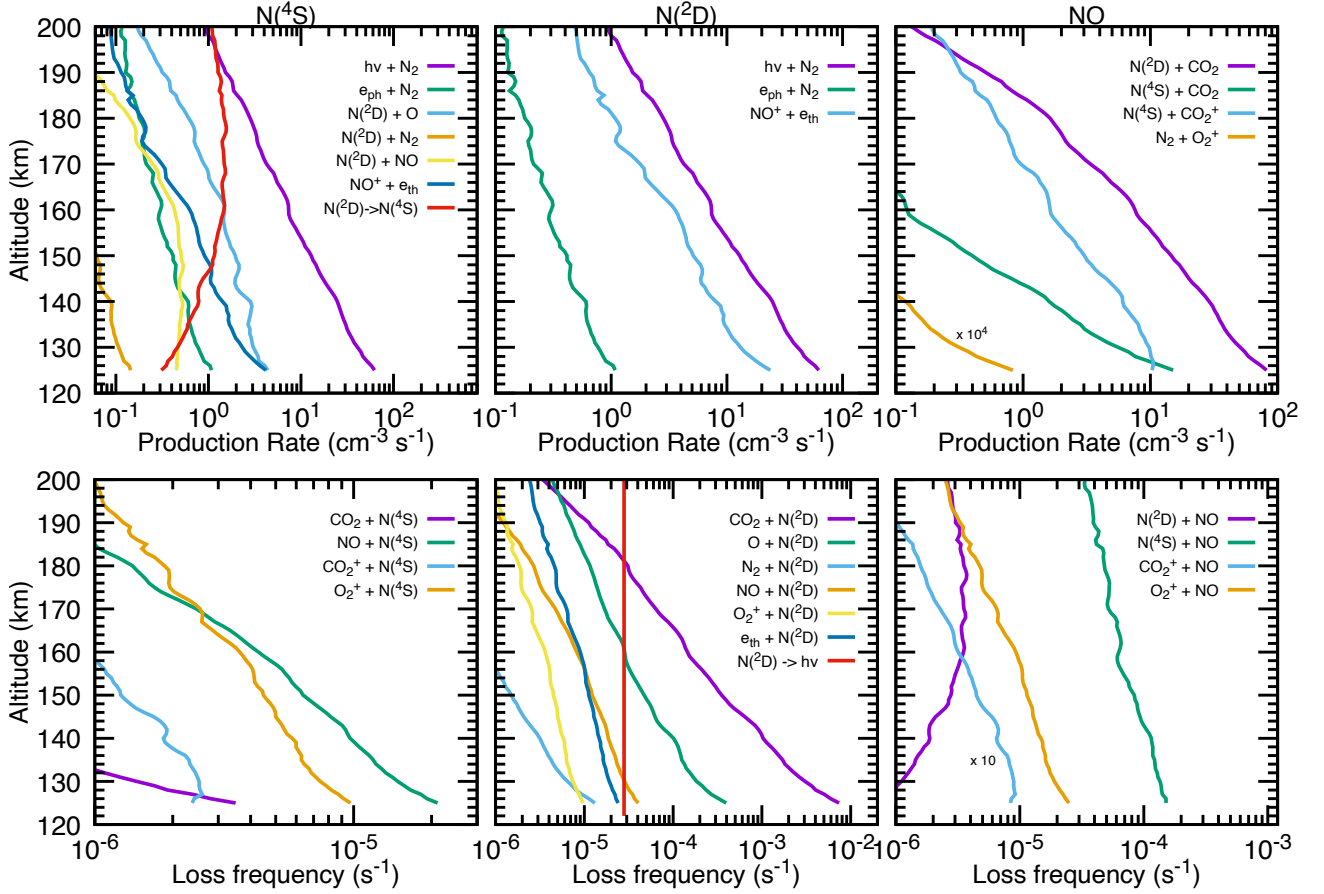


Figure 2: Various modelled formation (top panels) and destruction (bottom panels) processes for $N(^4S)$, $N(^2D)$ and NO in the Martian upper atmosphere for orbit #5947 during MAVEN deep dip 8 campaign. $h\nu$, e_{ph} , and e_{th} represent the solar photon, photoelectron, and thermal electron, respectively. Production rate of NO via N_2 and O_2^+ is plotted after multiplying by a factor of 10^4 . The reaction profile CO_2^+ and NO , which is a loss frequency profile of NO , is plotted after multiplying by a factor of 10.

nightside solar wind electron precipitation. The present study has several advances over Cui et al. (2020) in that (1) our calculations are made over a broad altitude range of 120 - 200 km to provide the vertical distribution of NO for deep dip 8 and 9 campaigns; (2) we emphasize the dayside variability in NO density driven by the variability of the background atmosphere, especially in terms of the CO_2 and N_2 densities, rather than the mean diurnal variability focused by Cui et al. (2020); (3) we also estimate the $NO(1,0)$ gamma band emission such that our results could be directly compared to the MAVEN IUVS limb observations. By comparing our modelled NO density profiles with Cui et al. (2020) calculations, we find that our calculated densities are smaller by a factor 2 to 3. This difference could be due to the different prevailed conditions in the Martian upper atmosphere during deep dip 2, 8 and 9 campaigns. Moreover, Cui et al. (2020) account for local time variability of neutral species in their calculations which is not the case in this work.

The calculations presented in Figure 2 show that the odd nitrogen species, which are primarily produced from the photodissociation of N_2 , initiate the formation of NO via collisions with CO_2 , and further interaction of these species

with NO subsequently recycles the N_2 in the Martian upper atmosphere (see chemical reactions R1, R8, R15 and R16 in Table 2). So it should be noticed that besides variation in CO_2 and N_2 densities, the NO density in the Martian upper atmosphere depends significantly on chemical reactions particularly R1 and R8, which are respective major production and loss channels initiated by photodissociation of N_2 . However, the calculations presented in figure 2 suggest that the NGIMS/MAVEN measured major neutral and ion densities (CO_2 , N_2 , and O_2^+) along with a few major chemical reactions are sufficient to determine the NO density in the altitude range 120 to 200 km, rather than using a complex chemical network.

The difference between our calculated odd nitrogen species density profiles and Fox (2004) modelled values, which is about a factor of 2 to 5, is mainly due to the change in input CO_2 and N_2 densities (see Figures 1 and 3). But our modelled NO density profile in the altitude range 120 to 200 km is closer to the Fox (2004) calculation (with a factor of 2 difference), which suggests that NO is strongly controlled by photochemical reactions rather than transport in the upper atmosphere. Time scales of odd nitrogen

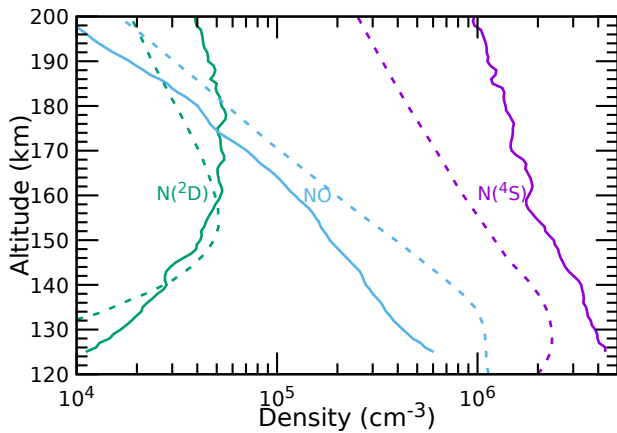


Figure 3: Modelled $N(^4S)$, $N(^2D)$, and NO densities in the Martian upper atmosphere for orbit #5947 of MAVEN deep dip 8 campaign. The dashed curves with corresponding colours represent the modelled density profiles from Fox (2004) for solar minimum condition.

species as determined by Cui et al. (2020) also suggest that NO is under photochemical equilibrium for the altitudes up to 180 km and above which chemical diffusion significantly controls its density (see Fig. 1d in Cui et al., 2020). Moreover, the agreement between our calculated NO densities for different orbits of deep dip 8 and 9 campaigns with the Stevens et al. (2019) modelled values for IUVS/MAVEN observation condition in the altitude range 120 to 160 km also supports our approach that NO can be derived from the NGIMS/MAVEN measured CO_2 and N_2 densities and also by considering the major photochemical reactions (see Figure 6).

NO density in the Martian upper atmosphere is significantly driven by photochemical reactions as well as local neutral densities of CO_2 and N_2 . Our calculations in Figure 2 show that below 170 km, the chemical cycle of NO mainly depends on density distribution of N_2 and CO_2 in the Martian upper atmosphere. Hence, the variation in the measured densities of these species directly can impact the modelled NO number density. As explained before, the variability in the MAVEN measured CO_2 and N_2 densities is directly linked to the NO density in the Martian upper atmosphere (see solid and dashed curves in Fig. 7) The higher volume mixing ratios of N_2 leads to the larger formation rate of dissociative products $N(^4S)$ and $N(^2D)$ and eventually can produce more NO . Since the major production source of NO is via collisional reactions between $N(^2D)$ with CO_2 , the variation in local CO_2 density can also control the NO density. The ambient density variation presented in the Figure 7 show that during deep dip 8 and 9 campaigns both CO_2 and N_2 densities varied by a factor of 5 or more in the Martian upper atmosphere which results in the variation in our calculated NO densities. The calculations done by Cui et al. (2020) for deep dip 2 campaign show that the diurnal variation in NO , $N(^4S)$ and $N(^2D)$ at the reference altitude 160 km is due to ambient N_2 mixing ratio at 160 km. But the calcu-

lations presented in this work show that besides the variation in N_2 volume mixing ratio, the change in CO_2 density also plays an important role in determining the NO density in the Martian upper atmosphere.

As shown in Figure 6, our calculated NO number densities around 125 km, for deep dip 8 and dip 9 campaigns, are consistent with the IUVS/MAVEN measurements and also with the modelled density profiles in the altitude range 120–160 km. It can be noticed in this figure that at 125 km altitude, the calculated NO number density varies by a factor of about 5 over the both deep dip campaigns, which is mainly due to the local variation in the measured CO_2 and N_2 densities. The earlier MAVEN deep dip campaigns also reveal that there is a variability in the measured neutrals and ions in the Martian upper atmosphere (Bougher et al., 2015b). Small scale structures in the NGIMS/MAVEN observed neutral and ion densities are linked to wave activity in the upper atmosphere or solar wind interaction with ionosphere (England et al., 2017; Kopf et al., 2008). Williamson et al. (2019) also observed large scale amplitude perturbations in the measured densities of different species, which could be due to gravity waves. These observations suggest that dynamics in the upper atmosphere could significantly influence the neutral densities of N_2 and CO_2 , and subsequently affect the NO density in the Martian upper atmosphere.

Stevens et al. (2019) were able to analyze the IUVS/MAVEN observed NO γ limb intensity profiles for a small period of observation i.e., 6–8 April 2016. Based on the observed limb intensity, the NO number densities were retrieved from the observed spectra between the altitudes 80 to 128 km, above which the retrieval becomes very difficult due to the presence of intense CO Cameron band emissions. But our method of calculation is able to determine the NO number density profile from 120 to 200 km. Since the derivation of NO density at higher altitudes is difficult, we suggest that our approach can be used as a baseline to constrain the NO abundance in the sunlit Martian upper atmosphere for different MAVEN observational conditions. However, the MAVEN observations are limited up to periapsis altitude and it is difficult to compute the NO densities lower than 120 km altitude using this approach.

Stevens et al. (2019) modelled NO density for the IUVS/MAVEN observation period and found that their derived density is smaller by a factor of 5 compared to the earlier Viking observations for the altitudes below 100 km. They ascribed this discrepancy to the assumed collisional rate coefficient for the reaction between $N(^4S)$ and CO_2 , which is $1 \times 10^{-18} \text{ cm}^3 \text{ s}^{-1}$ instead of earlier Fox (2004) assumed value of $1 \times 10^{-16} \text{ cm}^3 \text{ s}^{-1}$. By using the rate coefficient as used by Fox (2004), our calculations in Figure 2 show that the contribution from $N(^4S)$ and CO_2 collisions is negligible to the total formation of NO for the altitudes above 120 km. By considering Stevens et al. (2019) assumed rate coefficient in our calculations, which is two orders of magnitude smaller compared to the value used in the present work, we find no change in the modelled

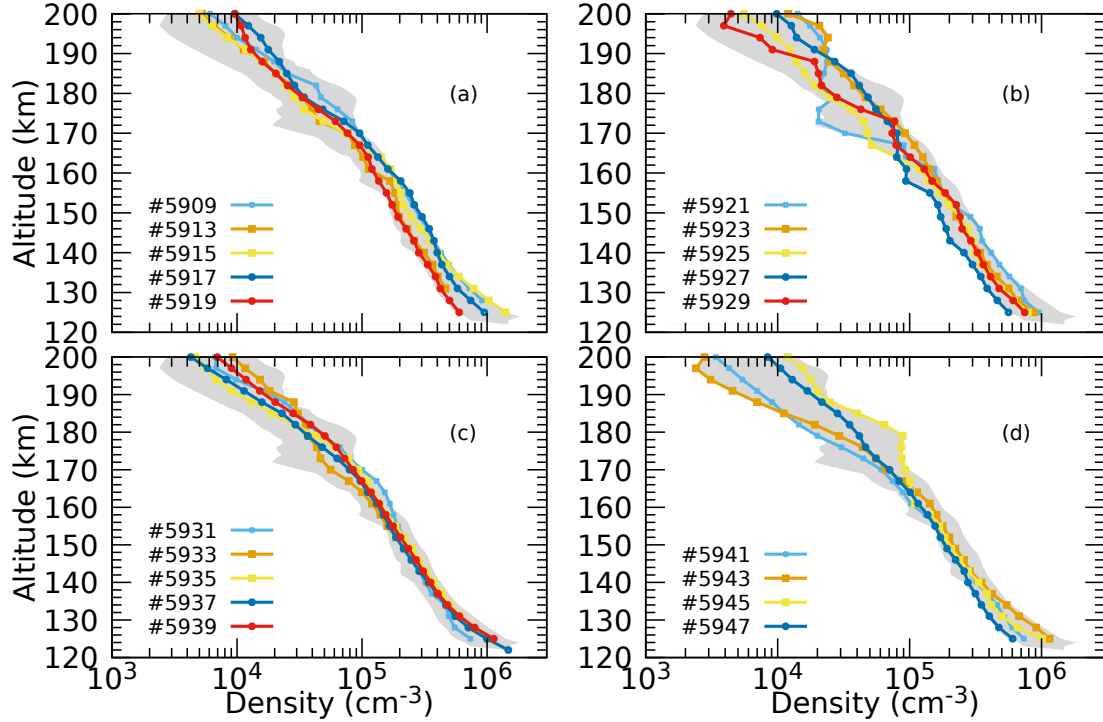


Figure 4: The modelled NO number density profiles for the various orbits of MAVEN deep dip 8 campaign. The Gray shaded area represents the variability in the calculated NO number density.

NO density profile. Thus, this calculation suggests that the contribution of $N(^4S)$ and CO_2 collisional reaction in the formation of NO can be neglected for the altitudes above 120 km.

Besides the observations of major neutral species, NGIMS/MAVEN also provides NO density measurements in the Martian upper atmosphere. But various observations show that the NGIMS/MAVEN measured NO densities are higher by an order of magnitude compared to IUVS/MAVEN derived values. This higher density is attributed to the recombination of N and O atoms inside the walls of mass spectrometer which produces additional NO. As Stevens et al. (2019) noticed, the effect of contamination in measuring the NO number density due to recombination of atomic oxygen and nitrogen cannot be neglected. By studying various factors associated in the calculation of NO density, Fox (2004) concluded that Viking 2 measurements may not be accurate. Hence, the instrumental bias during Viking 2 measurements could be the main reason for the discrepancy between the modelled and observation of NO densities. Thus, there remains a compelling need of new measurements of NO densities in the Martian upper atmosphere to reconcile this long-standing problem.

The high emission rate factor makes NO (1,0) transition as the brightest feature of γ band emission at the wavelength 214.9 nm compared to other transitions in the ultraviolet region. But this band emission is strongly obscured by CO (0,1) Cameron band emission (215.5 nm) due to proximity

in the wavelength and also due to its intensity. Using the derived NO densities, our calculated limb intensities during deep dip 8 and 9 campaigns are consistent with the mean value of IUVS/MAVEN measurement around 120 km (see Figure 10). However, it should be cautioned that the uncertainty in the measured limb radiance is large for the altitudes above 120 km (Stevens et al., 2019).

Fox (2004) has modelled NO number density for low solar activity condition, by assuming a downward flux of $-2 \times 10^7 \text{ cm}^{-2} \text{ s}^{-1}$ at lower boundary i.e., 80 km. Stevens et al. (2019) have reduced this downward flux value by two orders of magnitude to fit the IUVS/MAVEN retrieved NO density profiles. They also noticed that assumed transport flux can affect the shape of fitted profile only for altitudes below 100 km. But our calculated NO number densities around 120 km altitude are consistent with IUVS modelled profiles also supports the assumption that the transport has a minor role in determining NO number density in the altitude range 120–160 km (see Figure 6). Hence, we suggest that the NGIMS/MAVEN measured neutral and ion densities are suitable to study NO density and also its dayglow emission intensity for different seasonal conditions in the dayside upper atmosphere of Mars in this altitude range.

As earlier discussed, the intense CO Cameron band inhibits the measurement of NO emission intensity in the dayglow spectra. Our calculation in Figure 10 suggests that the emission intensity falls by an order of magnitude beyond 150 km, hence it is difficult to extract NO number density

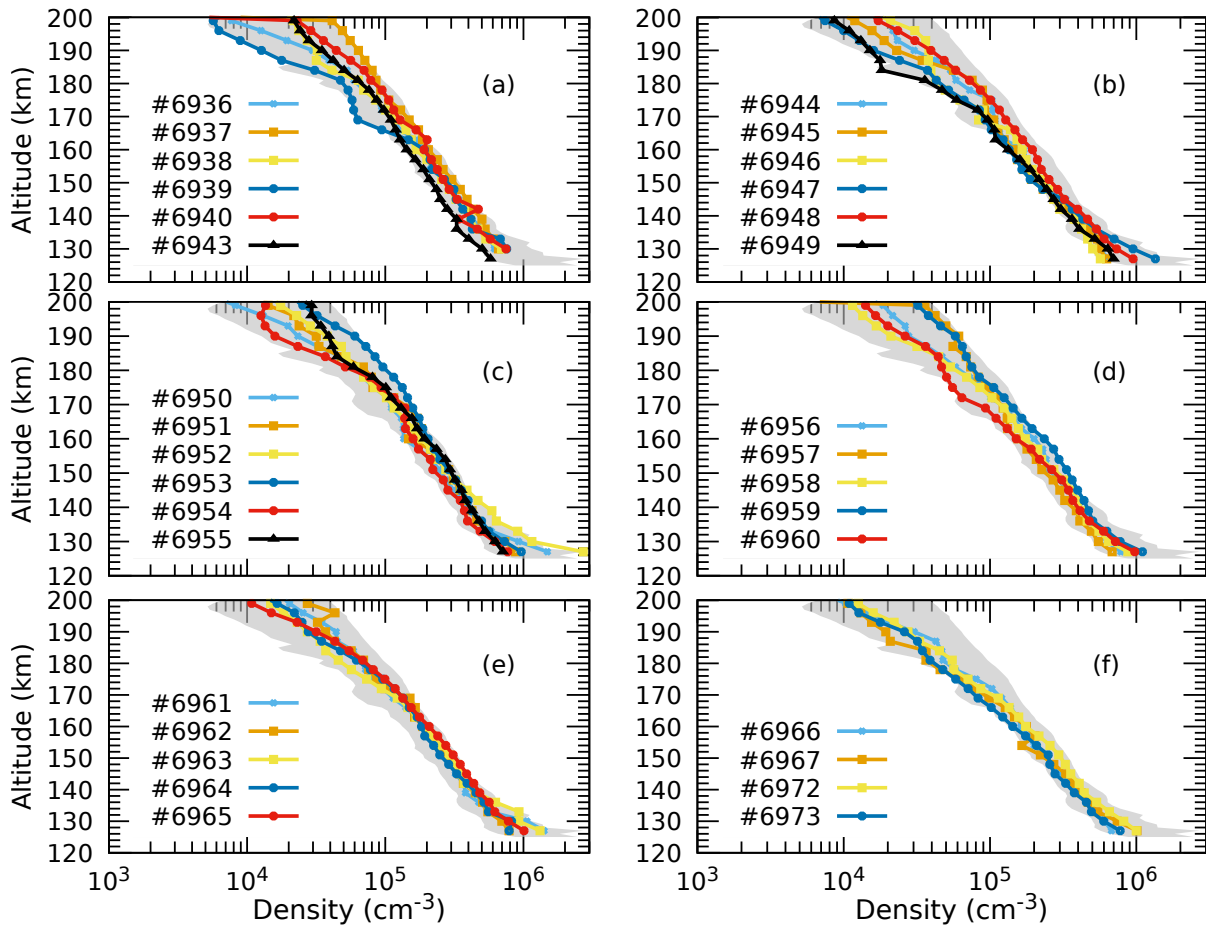


Figure 5: The calculated NO number density profiles for various orbits of MAVEN during Deep dip 9 campaign. The Gray shaded area represents the variability in the modelled NO number density.

from the faint NO γ band emission in the background of intense CO Cameron band emission. Hence, we suggest that the derivation of NO number density based on photochemistry and subsequently calculating its dayglow emission intensity can serve as a baseline while analysing the ongoing and upcoming IUVS/MAVEN observations. More such observations of NO dayglow emissions along with modelling studies are necessary to constrain its variability in the Martian upper atmosphere.

5. Summary and Conclusions

The in-situ NO density measurements are difficult to make in the Martian upper atmosphere because of its low abundance (more than 3 orders of magnitude compared to CO_2) and also highly reactive in nature. Moreover, the thermal recombination of atomic nitrogen and atomic oxygen inside the mass spectrometer also inhibits the accurate determination of NO density. Measurement of NO density from the remote dayglow observations is also difficult since its strongest ultraviolet emission feature, i.e., (1,0) gamma band, is severely obscured by the intense CO Cameron band (50 times higher in magnitude). By accounting for major chemical reactions and using the NGIMS/MAVEN

measured neutral and ion densities, we developed a photochemical model to study the photochemistry of NO in the Martian upper atmosphere. MAVEN's deep dip campaigns provide a unique opportunity to study NO photochemistry in the dayside Martian upper atmosphere at the altitudes as low as 120 km. By utilizing the NGIMS/MAVEN measured neutral and ion densities during MAVEN deep dip 8 and 9 campaigns in our model, we present a method to calculate NO number density in the dayside upper atmosphere of Mars. Using the modelled NO number density profiles we also calculated NO dayglow (1,0) γ band emission intensity. Our calculated NO number density profiles are consistent with the IUVS/MAVEN retrieved profile and also with the modelled values for IUVS observation conditions. We found that the calculated NO number density varies by a factor of 2–5 and consequently its dayglow intensity due to the variation in CO_2 and N_2 densities at around 120 km. Hence, we suggest that the present method of calculation serves as a baseline to estimate the NO number density and also its γ bands emission intensity under different seasonal and solar conditions in the dayside Martian upper atmosphere. Based on our calculations we suggest that future MAVEN deep dip and remote IUVS/MAVEN observations should be focused in the altitude region 120 and 130 km to

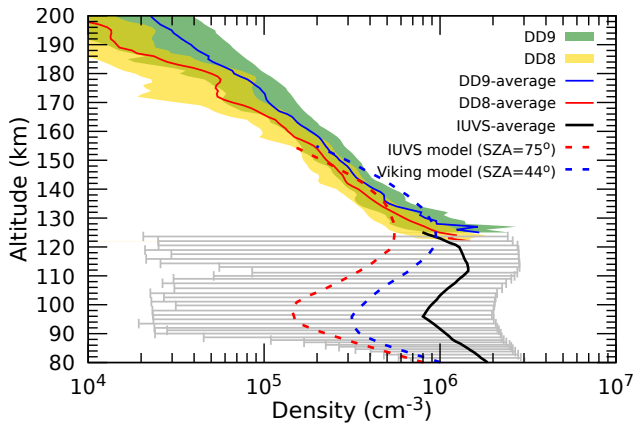


Figure 6: Comparison between the modelled and MAVEN deep dip 8 (solid red curve for the average), 9 (solid blue curve for the average) and IUVS/MAVEN (solid black curve) retrieved mean and Viking modelled at SZA 44° (blue-dashed curve) and IUVS modelled at SZA 75° (red-dashed curve) NO number density profiles in the Martian upper atmosphere. The yellow and green shaded areas represent the variability in calculated NO number density profiles during MAVEN deep dip 8 and 9 campaigns, respectively. The horizontal Gray error bars represent the digitized data of 1- σ variability about the mean value of the IUVS derived NO number density (taken from Stevens et al., 2019).

constrain the NO density in the Martian upper atmosphere. More observations of NO emissions along with modelling studies are necessary to fully comprehend the NO density distribution on the dayside upper atmosphere of Mars.

Acknowledgements

SR is supported by Department of Science and Technology (DST) with Innovation in Science Pursuit for Inspired Research (INSPIRE) faculty award [grant:dst/inspire/04/2016/002687], and he would like to thank Physical Research Laboratory for facilitating conducive research environment. He is a visiting researcher at Khalifa University during a part of this work. AB was J.C. Bose Fellow during the period of this work. A part of this work was done when MD was PDF at PRL and presently working at Maulana Azad National Institute of Technology Bhopal as an assistant professor.

Data Availability

This paper makes use of NGIMS/MAVEN measured neutral and ion number densities L2 data for deep dip 8 and 9 campaigns which has been accessed through the web link <https://pds-atmospheres.nmsu.edu>. The derived data generated in this research will be shared on reasonable request to the corresponding author.

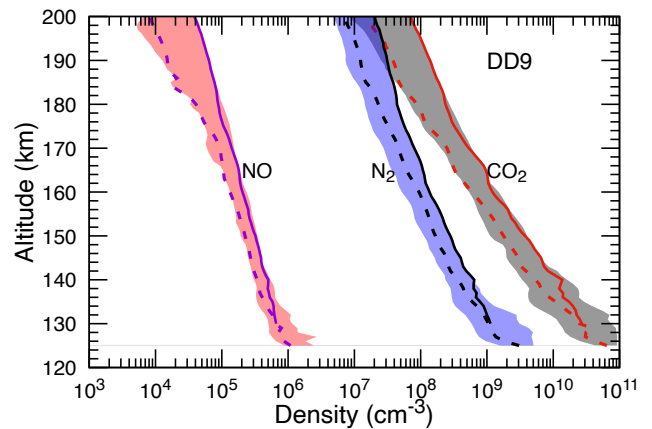
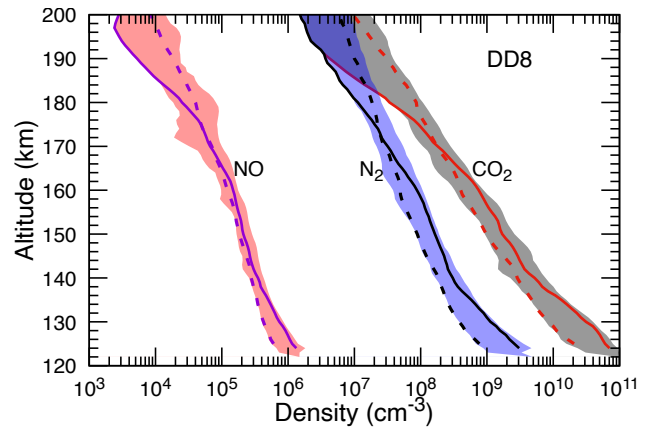


Figure 7: Variation in the modelled NO density due to the change in the NGIMS/MAVEN measured CO₂ and N₂ densities during the MAVEN deep dip 8 (top panel) and 9 (bottom panel) campaigns. The solid and dashed curves in the top panel (bottom panel) represent the corresponding number densities for orbits #5943 and #5947 (#6937 and #6949), respectively, for MAVEN deep dip 8 (9) campaign.

References

- Barth, C.A., 1964. Rocket Measurement of the Nitric Oxide Dayglow. *J. Geophys. Res.* 69, 3301–3303. doi:10.1029/JZ069i015p03301.
- Barth, C.A., Mankoff, K.D., Bailey, S.M., Solomon, S.C., 2003. Global observations of nitric oxide in the thermosphere. *Journal of Geophysical Research (Space Physics)* 108, 1027. doi:10.1029/2002JA009458.
- Benna, M., Elrod, M., 2018. Mars Atmosphere and Volatile Evolution (MAVEN) mission, Neutral Gas and Ion Mass Spectrometer (NGIMS), NGIMS PDS Software Interface Specification, Revision 1.9 Rev. 1.9.
- Berrington, K.A., Burke, P.G., 1981. Effective collision strengths for forbidden transitions in e-N and e-o scattering. *Planet. Space Sci.* 29, 377–381. doi:10.1016/0032-0633(81)90026-X.
- Bertaux, J.L., Leblanc, F., Perrier, S., Quemerais, E., Korabely, O., Dimarellis, E., Reberac, A., Forget, F., Simon, P.C., Stern, S.A., Sandel, B., 2005a. Nightglow in the Upper Atmosphere of Mars and Implications for Atmospheric Transport. *Science* 307, 566–569. doi:10.1126/science.1106957.
- Bertaux, J.L., Leblanc, F., Witasse, O., Quemerais, E., Liliensten, J., Stern, S.A., Sandel, B., Korabely, O., 2005b. Discovery of an aurora on Mars. *Nature* 435, 790–794. doi:10.1038/nature03603.
- Bhardwaj, A., 1999. On the role of solar EUV, photoelectrons, and auroral electrons in the chemistry of C(1D) and the production of C I 1931 Å in the inner cometary coma: A case for comet P/Halley. *J. Geophys. Res.* 104, 1929 – 1942. doi:10.1029/1998JE900004.

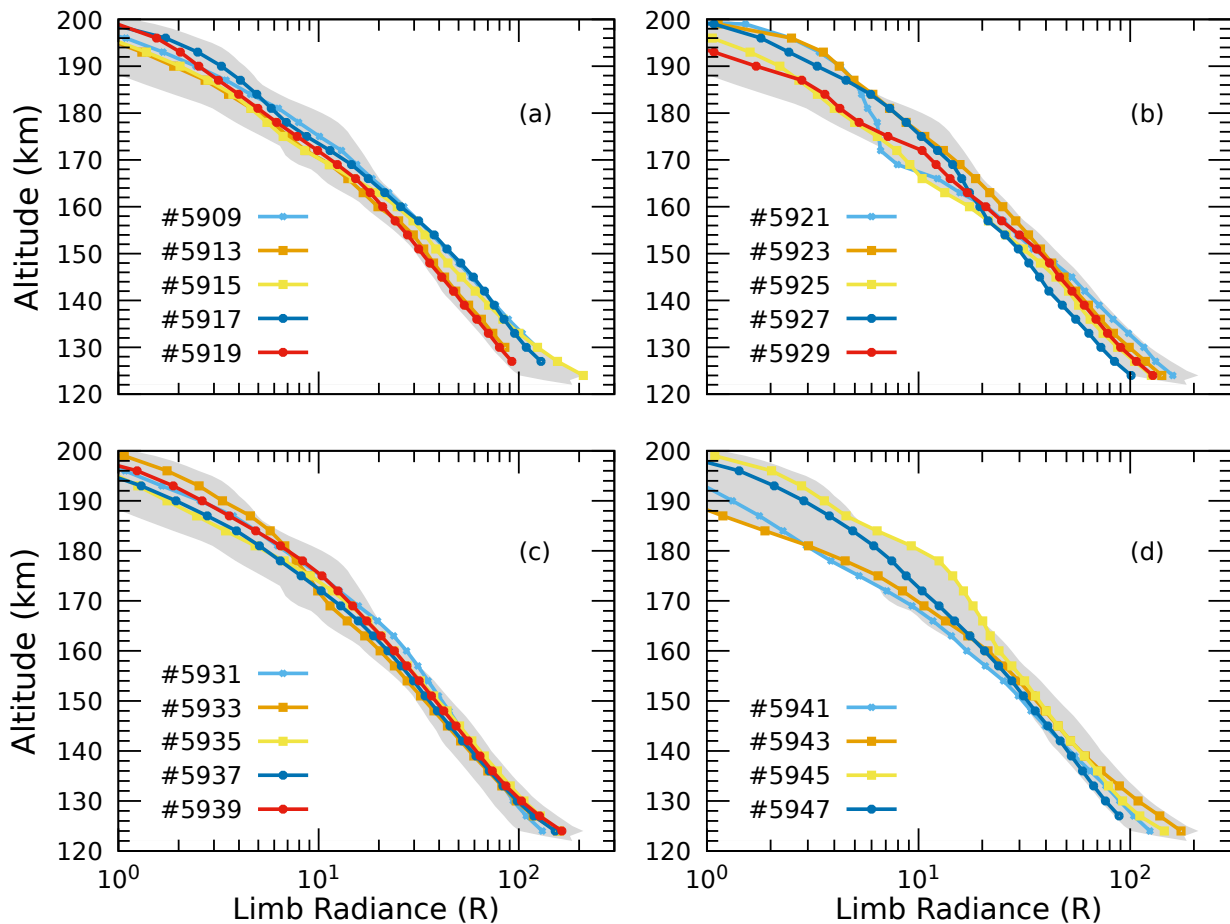


Figure 8: Modelled limb radiance profiles for Nitric oxide (NO) 1-0 γ emission for the MAVEN Deep dip 8 campaign. The Gray shaded area represents the variability in the calculated NO (1-0) γ intensity.

- Bhardwaj, A., Haider, S.A., alal, R.P., 1996. Production and emissions of atomic carbon and oxygen in the inner coma of comet 1P/Halley: Role of electron impact. *Icarus* 120, 412 – 430. doi:10.1006/icar.1996.0061.
- Bhardwaj, A., Haider, S.A., Singhal, R.P., 1990. Auroral and photoelectron fluxes in cometary ionospheres. *ICARUS* 85, 216–228. doi:10.1016/0019-1035(90)90112-M.
- Bhardwaj, A., Jain, S.K., 2013. CO Cameron band and CO₂+ UV doublet emissions in the dayglow of Venus: Role of CO in the Cameron band production. *Journal of Geophysical Research (Space Physics)* 118, 3660–3671. doi:10.1002/jgra.50345, arXiv:1305.6139.
- Bhardwaj, A., Thampi, S.V., Das, T.P., Dhanya, M.B., Naik, N., Vajja, D.P., Pradeepkumar, P., Sreelatha, P., Abhishek J., K., Thampi, R.S., Yadav, V.K., Sundar, B., Nand i, A., Padmanabhan, G.P., Aliyas, A.V., 2017. Observation of suprathermal argon in the exosphere of Mars. *Geophys. Res. Lett.* 44, 2088–2095. doi:10.1002/2016GL072001.
- Bhardwaj, A., Thampi, S.V., Das, T.P., Dhanya, M.B., Naik, N., Vajja, D.P., Pradeepkumar, P., Sreelatha, P., Supriya, G., Abhishek J., K., Mohankumar, S.V., Thampi, R.S., Yadav, V.K., Sundar, B., Nandi, A., Padmanabhan, G.P., Aliyas, A.V., 2016. On the evening time exosphere of Mars: Result from MENCA aboard Mars Orbiter Mission. *Geophys. Res. Lett.* 43, 1862–1867. doi:10.1002/2016GL067707.
- Bharti, G., Sunil Krishna, M.V., Singh, V., 2019. Radiative cooling due to NO at 5.3 μ m emission as observed by TIMED/SABER over Asian sector. *Advances in Space Research* 64, 1989–2001. doi:10.1016/j.asr.2019.07.016.
- Bougher, S., Jakosky, B., Halekas, J., Grebowsky, J., Luhmann, J., Mahaffy, P., Connerney, J., Eparvier, F., Ergun, R., Larson, D., McFadden, J., Mitchell, D., Schneider, N., Zurek, R., Mazelle, C., Andersson, L., Andrews, D., Baird, D., Baker, D.N., Bell, J.M., Benna, M., Brain, D., Chaffin, M., Chamberlin, P., Chaufray, J.Y., Clarke, J., Collinson, G., Combi, M., Crary, F., Cravens, T., Crismani, M., Curry, S., Curtis, D., Deighan, J., Delory, G., Dewey, R., DiBraccio, G., Dong, C., Dong, Y., Dunn, P., Elrod, M., England, S., Eriksson, A., Espley, J., Evans, S., Fang, X., Fillingim, M., Fortier, K., Fowler, C.M., Fox, J., Gröller, H., Guzewich, S., Hara, T., Harada, Y., Holsclaw, G., Jain, S.K., Jolitz, R., Leblanc, F., Lee, C.O., Lee, Y., Lefevre, F., Lillis, R., Livi, R., Lo, D., Ma, Y., Mayyasi, M., McClintock, W., McEnulty, T., Modolo, R., Montmessin, F., Morooka, M., Nagy, A., Olsen, K., Peterson, W., Rahmatii, A., Ruhunusiri, S., Russell, C.T., Sakai, S., Sauvaud, J.A., Seki, K., Steckiewicz, M., Stevens, M., Stewart, A.I.F., Stiepen, A., Stone, S., Tenishev, V., Thiemann, E., Tolson, R., Toubanc, D., Vogt, M., Weber, T., Withers, P., Woods, T., Yelle, R., 2015a. Early MAVEN Deep Dip campaign reveals thermosphere and ionosphere variability. *Science* 350, 0459. doi:10.1126/science.aad0459.
- Bougher, S.W., Pawlowski, D., Bell, J.M., Nelli, S., McDunn, T., Murphy, J.R., Chizek, M., Ridley, A., 2015b. Mars Global Ionosphere-Thermosphere Model: Solar cycle, seasonal, and diurnal variations of the Mars upper atmosphere. *Journal of Geophysical Research (Planets)* 120, 311–342. doi:10.1002/2014JE004715.
- Cox, C., Saglam, A., Gérard, J.C., Bertaux, J.L., González-Galindo, F., Leblanc, F., Reberac, A., 2008. Distribution of the ultraviolet nitric oxide Martian night airglow: Observations from Mars Express and comparisons with a one-dimensional model. *Journal of Geophysical Research (Planets)* 113, E08012. doi:10.1029/2007JE003037.
- Cui, J., Fu, M.H., Ren, Z.P., Gu, H., Guo, J.H., Wu, X.S., Wu, Z.P., Lai, H.R., Wei, Y., 2020. Nitric Oxide Abundance in the Martian Thermosphere and Its Diurnal Variation. *Geophys. Res. Lett.* 47, e87252. doi:10.1029/2020GL087252.

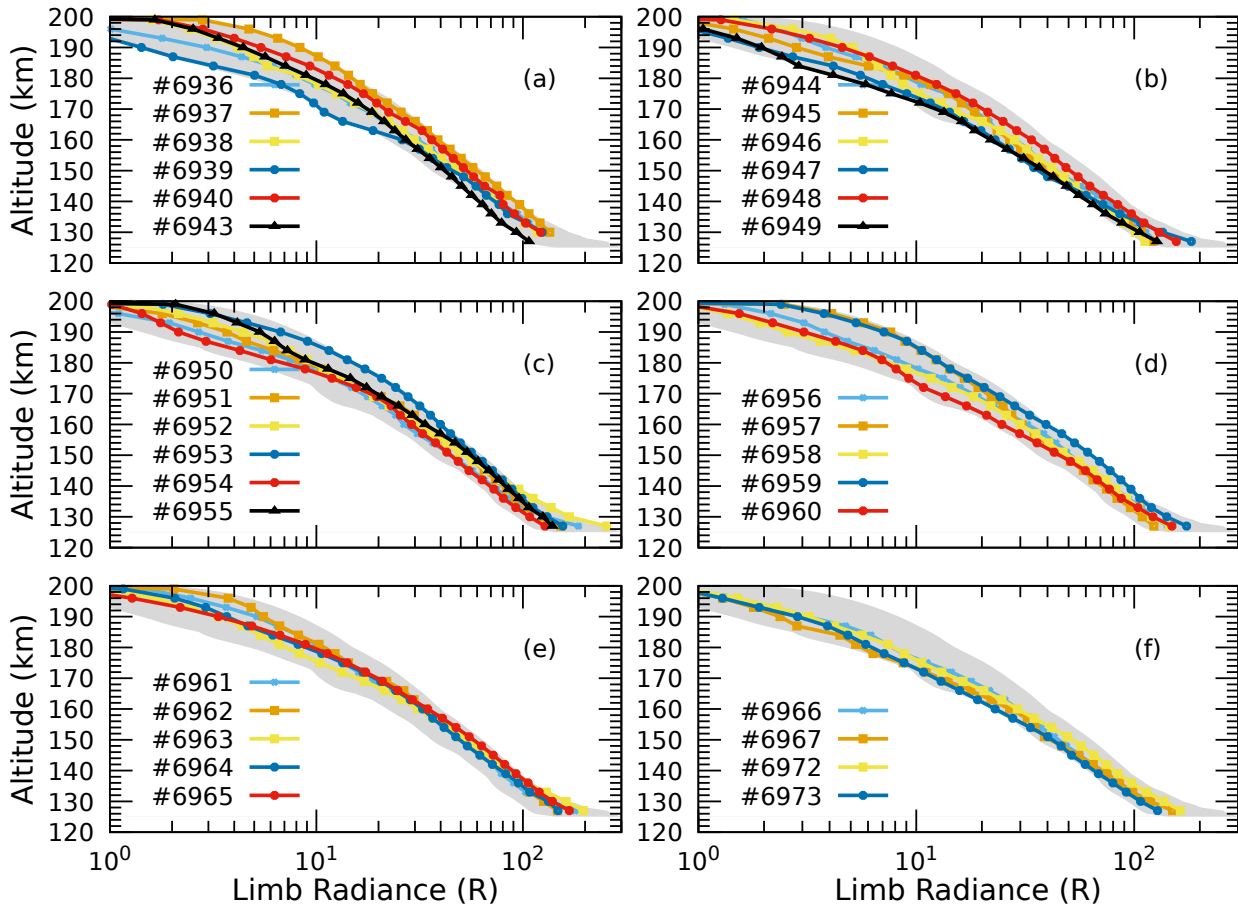


Figure 9: Modelled limb radiance profile of Nitric oxide (NO) emission for the MAVEN deep dip 9 campaign. The Gray shaded area represents the variability in the calculated NO (1-0) γ intensity.

England, S.L., Liu, G., Yiğit, E., Mahaffy, P.R., Elrod, M., Benna, M., Nakagawa, H., Terada, N., Jakosky, B., 2017. MAVEN NGIMS observations of atmospheric gravity waves in the Martian thermosphere. *Journal of Geophysical Research (Space Physics)* 122, 2310–2335. doi:10.1002/2016JA023475.

Eparvier, F.G., Barth, C.A., 1992. Self-absorption theory applied to rocket measurements of the nitric oxide (1,0) γ band in the daytime thermosphere. *J. Geophys. Res.* 97, 13723–13731. doi:10.1029/92JA00993.

Ergun, R.E., Morooka, M.W., Andersson, L.A., Fowler, C.M., Delory, G.T., Andrews, D.J., Eriksson, A.I., McEnulty, T., Jakosky, B.M., 2015. Dayside electron temperature and density profiles at Mars: First results from the MAVEN Langmuir probe and waves instrument. *Geophys. Res. Lett.* 42, 8846–8853. doi:10.1002/2015GL065280.

Fell, C., Steinfeld, J.I., Miller, S., 1990. Quenching of N(2D) by O(3P). *J. Chemphys.* 92, 4768–4777. doi:10.1063/1.457694.

Fox, J.L., 1993. The production and escape of nitrogen atoms on Mars. *J. Geophys. Res.* 98, 3297–3310. doi:10.1029/92JE02289.

Fox, J.L., 2004. Response of the Martian thermosphere/ionosphere to enhanced fluxes of solar soft X rays. *J. Geophys. Res. (Space Physics)* 109, A11310. doi:10.1029/2004JA010380.

Fox, J.L., Sung, K.Y., 2001. Solar activity variations of the Venus thermosphere/ionosphere. *J. Geophys. Res. (Space Physics)* 106, 21305–21336. doi:10.1029/2001JA000069.

Gagné, M.E., Bertaux, J.L., González-Galindo, F., Melo, S.M.L., Montmessin, F., Strong, K., 2013. New nitric oxide (NO) nightglow measurements with SPICAM/MEx as a tracer of Mars upper atmosphere circulation and comparison with LMD-MGCM model prediction: Evidence for asymmetric hemispheres. *Journal of Geophysical Research (Planets)* 118, 2172–2179. doi:10.1002/jgre.20165.

Goldan, P.D., Schmeltekopf, A.L., Fehsenfeld, F.C., Schiff, H.I., Ferguson, E.E., 1966. Thermal Energy Ion-Neutral Reaction Rates. II. Some Reactions of Ionospheric Interest. *J. Chemphys.* 44, 4095–4103. doi:10.1063/1.1726588.

González-Galindo, F., Forget, F., López-Valverde, M.A., Angelats i Coll, M., Millour, E., 2009. A ground-to-exosphere Martian general circulation model: 1. Seasonal, diurnal, and solar cycle variation of thermospheric temperatures. *Journal of Geophysical Research (Planets)* 114, E04001. doi:10.1029/2008JE003246.

Herron, J.T., 1999. Evaluated Chemical Kinetics Data for Reactions of N(2D) N(2P), and N2(A3Sigma+u) in the Gas Phase. *Journal of Physical and Chemical Reference Data* 28, 1453–1483. doi:10.1063/1.556043.

Jain, S.K., Bhardwaj, A., 2011. Model calculation of N2 Vegard-Kaplan band emissions in Martian dayglow. *Journal of Geophysical Research (Planets)* 116, E07005. doi:10.1029/2010JE003778, arXiv:1108.0490.

Jain, S.K., Bhardwaj, A., 2012. Impact of solar EUV flux on CO Cameron band and CO2 UV doublet emissions in the dayglow of Mars. *Planetary and Space Science* 64, 110–122.

Kopf, A.J., Gurnett, D.A., Morgan, D.D., Kirchner, D.L., 2008. Transient layers in the topside ionosphere of Mars. *Geophys. Res. Lett.* 35, L17102. doi:10.1029/2008GL034948.

Krasnopolsky, V.A., 1993. Photochemistry of the Martian atmosphere (mean conditions). *ICARUS* 101, 313–332. doi:10.1006/icar.1993.1027.

Mahaffy, P.R., Benna, M., King, T., Harpold, D.N., Arvey, R., Barciniak, M., Bendt, M., Carrigan, D., Errigo, T., Holmes, V., Johnson, C.S., Kellogg, J., Kimvilakani, P., Lefavor, M., Hengemihle, J., Jaeger, F., Lyness, E., Maurer, J., Melak, A., Noreiga, F., Noriega, M., Patel, K., Prats, B., Raaen, E., Tan, F., Weidner, E., Gundersen, C., Battel, S., Block, B.P., Arnett, K., Miller, R., Cooper, C., Edmonson, C., Nolan,

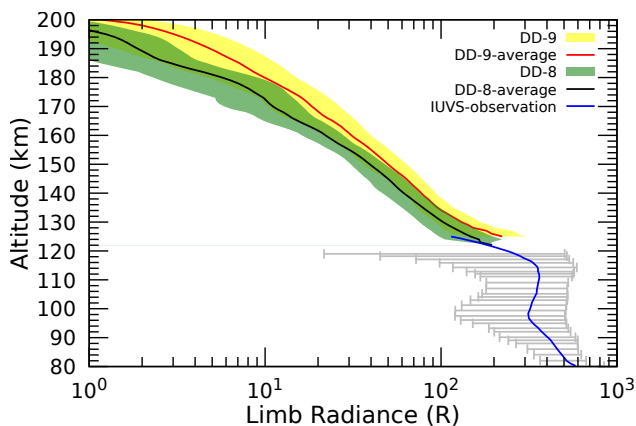


Figure 10: Comparison between the modelled and the IUVS/MAVEN observed NO (1,0) γ band limb intensity profiles. The black and red curves represent the calculated average NO (1,0) γ band limb intensity for deep dip 8 and 9 missions respectively. Blue curve and gray errors bars represents the observed average IUVS/MAVEN dayglow profile and 1- σ uncertainty associated with observation, respectively (taken from Stevens et al., 2019). Green and yellow shaded areas represent the variability in the calculated NO (1,0) γ band limb intensity for deep dip 8 and 9 missions, respectively.

- Williamson, H.N., Johnson, R.E., Leclercq, L., Elrod, M.K., 2019. Large amplitude perturbations in the Martian exosphere seen in MAVEN NGIMS data. *Icarus* 331, 110–115. doi:10.1016/j.icarus.2019.05.020.
- Withers, P., 2006. Mars Global Surveyor and Mars Odyssey Accelerometer observations of the Martian upper atmosphere during aerobraking. *Geophys. Res. Lett.* 33, L02201. doi:10.1029/2005GL024447.

- J.T., 2015. The Neutral Gas and Ion Mass Spectrometer on the Mars Atmosphere and Volatile Evolution Mission. *Space Science Rev.* 195, 49–73. doi:10.1007/s11214-014-0091-1.
- Matsuoka, S., Nakamura, H., Tamura, T., 1981. Ion-molecule reactions of N_3^+ , N_4^+ , O_2^+ , and NO_2^+ in nitrogen containing traces of oxygen. *J. Chem. Phys.* 75, 681–689. doi:10.1063/1.442108.
- McElroy, D., Walsh, C., Markwick, A.J., Cordiner, M.A., Smith, K., Millar, T.J., 2013. The UMIST database for astrochemistry 2012. *A&A* 550, A36. doi:10.1051/0004-6361/201220465.
- McElroy, M.B., Kong, T.Y., Yung, Y.L., Nier, A.O., 1976. Composition and structure of the Martian upper atmosphere - Analysis of results from Viking. *Science* 194, 1295–1298. doi:10.1126/science.194.4271.1295.
- Nier, A.O., McElroy, M.B., 1977. Composition and structure of Mars' upper atmosphere - Results from the neutral mass spectrometers on Viking 1 and 2. *J. Geophys. Res.* 82, 4341–4349. doi:10.1029/JS082i028p04341.
- Norton, R.B., Barth, C.A., 1970. Theory of nitric oxide in the Earth's atmosphere. *J. Geophys. Res.* 75, 3903. doi:10.1029/JA075i019p03903.
- Raghuram, S., Bhardwaj, A., 2020. CO+ first-negative band emission: A tracer for CO in the Martian upper atmosphere. [arXiv:2005.09473](https://arxiv.org/abs/2005.09473)doi:10.1051/0004-6361/202038147, [arXiv:2005.09473](https://arxiv.org/abs/2005.09473).
- Scott, G.B.I., Fairley, D.A., Freeman, C.G., McEwan, M.J., Anicich, V.G., 1998. Gas-phase reactions of some positive ions with atomic and molecular nitrogen. *J. Chem. Phys.* 109, 9010–9014. doi:10.1063/1.477571.
- Stevens, M.H., Sisikind, D.E., Evans, J.S., Fox, J.L., Deighan, J., Jain, S.K., Schneider, N.M., 2019. Detection of the Nitric Oxide Dayglow on Mars by MAVEN/IUVS. *J. Geophys. Res.* 124, 1 – 12. doi:10.1029/2019JE005945.
- Tachiev, G.I., Froese Fischer, C., 2002. Breit-Pauli energy levels and transition rates for nitrogen-like and oxygen-like sequences. *A&A* 385, 716–723. doi:10.1051/0004-6361:20011816.
- Vejby-Christensen, L., Kella, D., Pedersen, H.B., Andersen, L.H., 1998. Dissociative recombination of NO^+ . *Physical Rev. A* 57, 3627–3634. doi:10.1103/PhysRevA.57.3627.
- Vogt, M.F., Withers, P., Fallows, K., Andersson, L., Girazian, Z., Mahaffy, P.R., Benna, M., Elrod, M.K., Connerney, J.E.P., Espley, J.R., Eparvier, F.G., Jakosky, B.M., 2017. MAVEN observations of dayside peak electron densities in the ionosphere of Mars. *Journal of Geophysical Research (Space Physics)* 122, 891–906. doi:10.1002/2016JA023473.